crystals

MDPI

Article

The Behavior of Water in Orthoclase Crystal and Its Implications for Feldspar Alteration

Hongyan Zuo [1], Rui Liu [2] and Anhuai Lu [3,*]

[1] State Key Laboratory of Lunar and Planetary Sciences, Macau University of Science and Technology, Taipa, Macau 999078, China; hyzuo2014@gmail.com
[2] School of Prospecting and Survey, Jilin Oil Shale Drilling and Environmental Protecting Laboratory, Changchun Institute of Technology, Changchun 130021, China; gglr984@sohu.com
[3] Beijing Key Laboratory of Mineral Environmental Function, School of Earth and Space Sciences, Peking University, Beijing 100871, China
* Correspondence: ahlu@pku.edu.cn

Abstract: The phenomenon of feldspar alteration that occurs in the interior of feldspar crystals remains poorly understood. We observed experimentally that water can go into orthoclase crystals under pressures of up to 600 MPa at room temperature. With increasing pressure, the FTIR spectra of colorless orthoclase show a sharp increase in integral absorbance from 1.50 cm^{-1} to 14.54 cm^{-1} and normalized integral absorbance from 120 cm^{-2} to 1570 cm^{-2}; the pink orthoclase saturates quickly with no significant change in either the integral absorbance or normalized integral absorbance. The different responses to the pressure between colorless orthoclase and pink orthoclase might be related to the K content in the structure. Moreover, FTIR spectra at atmospheric pressure collected in different crystallography directions show different absorbance intensities, which illustrates the characteristic of preferred crystallographic orientations. These results reveal that H_2O molecules can occur as structural constituents entering the crystallographic channels of alkali feldspar crystals, preferentially along (001) orientation. These findings provide clues into the mechanism of feldspar alteration occurring in the interior of feldspar crystals, as well as the formation of micropores and microstructure in feldspar minerals. This study also provides important insights into the behavior of water molecules in nominally anhydrous minerals in the upper crust of the Earth.

Keywords: orthoclase crystal; ultra-microchannel; water; feldspar alteration; sericitization

Citation: Zuo, H.; Liu, R.; Lu, A. The Behavior of Water in Orthoclase Crystal and Its Implications for Feldspar Alteration. *Crystals* **2022**, *12*, 1042. https://doi.org/10.3390/cryst12081042

Academic Editor: Vladislav V. Gurzhiy

Received: 14 June 2022
Accepted: 24 July 2022
Published: 27 July 2022

1. Introduction

Feldspars make up more than 50% of the Earth's crust. Thus, feldspar alteration is ubiquitous within the crust [1,2]. The ideal formula of a feldspar is MT_4O_8 [3]. Feldspar has a three-dimensional framework of corner-sharing AlO_4 and SiO_4 tetrahedra [4]. The degree of Al/Si order in the tetrahedral sites in feldspars is related to the formation conditions of the minerals [5,6]. The framework structure of feldspars is based on the linked TO_4 tetrahedra [4,7]. In the framework structure, the oxygen atoms lie at the corners of the tetrahedron centered by Al or Si atoms. All oxygen atoms are shared by two T (Al or Si) atoms to form a framework like a three-dimensional network [8]. The substitution of Si (+4) with Al (+3) in the tetrahedron makes the structure's charge imbalanced. Thus, the irregularly shaped cavities formed by the framework can be occupied by the large M cations to obtain a charge balance. Moreover, a special characteristic of the feldspar structure is the occurrence of chains of tetrahedra that are cross-linked in a special way to form crankshaft and elliptical rings of tetrahedra [9–11].

In the structure of feldspar, the eight-membered rings of tetrahedra overlap each other, forming ultra-microchannels of 0.1 nm × 0.1 nm width along (100), while the six-membered rings of tetrahedra form elliptical ultra-microchannels of 0.1 nm × 0.3 nm width along (001) [12]. However, it is more complex along (101). They are constructed with tetragonal

TO_4 sharing the apex, forming the double-crankshaft chain. The double chains connect to form two kinds of channels along (101), in which the aperture of six-membered rings is 0.1 nm × 0.1 nm. Another aperture formed by ten tetragonal TO_4 sharing the apex is 0.15 nm × 0.67 nm [12]. The 10-membered elliptical ring is the largest channel in feldspar, and alkali or alkaline-earth cations such as Na^+, K^+, Ca^{2+}, and Ba^{2+} or even Pb^{2+}, Cd^{2+}, and Mg^{2+} can occupy this type of channel [12,13]. The overall structural states of feldspars (including obliquity, triclinicity, and degree of disorder) are very complex and may correlate to the petrogenesis of their containing rocks [14–16].

Feldspar minerals can develop microcracks. These microcracks are mainly in three ranges: 1.0–2.0 nm, 10–15 nm, and >50 nm. Microcracks, including micropores and microstructures, are contributors to the processes of crystals coarsening and deuteric or hydrothermal alteration [17]. The microcracks, together with cleavage, twinning, and the grain-to-grain boundary, are thought to be responsible for weathering and alteration. Feldspar alteration is a consistent concern for geologists, mineralogists, and environment scientists [1,18–22]. Interestingly, fine-grained sericite was reported to occur as an alteration product in the interior of feldspar crystals [23–26]. However, the alteration that occurs in the interior of feldspar crystals is not fully understood yet. Given the fact that the diameter of water molecule is only 0.276 nm, water might be able to go through the ultra-microchannels.

In this work, we focus on the behavior of water going into the ultra-microchannels of feldspars. Two types of feldspars are selected for high-pressure experiments up to 600 MPa and oriented FTIR analysis. In situ Raman spectroscopic measurement in a cubic zirconia anvil cell was conducted in high-pressure experiments. FTIR analysis was used to detect the species and content of hydrogen (OH^- and H_2O) in feldspars. The results of this study provide important insights into feldspar alteration and the behavior of water molecules in nominally anhydrous minerals in the upper crust of the Earth.

2. Materials and Methods

2.1. Materials

Colorless and pink feldspars were collected from granite in the Barkol area in eastern Junggar, Xinjiang. The compositions of these feldspars were measured with electron probe microanalysis (EPMA), and both the colorless and pink samples were determined to be orthoclase (hereafter called colorless orthoclase and pink orthoclase; contents in Table 1 refer to average analysis). Natural crystals of albite, rhodonite, plagioclase, orthoclase, pyrope, almandine, anhydride, and benitoite were used as EPMA standards. Multipoint measurements were carried out, and the total standard deviation is less than 0.3%. The mineralogical composition of the studied materials was further confirmed by transmission electron microscopy and selected area electron diffraction (Figure 1). The lattice image of the colorless orthoclase shows two d-spacings of 0.59 nm and 0.65 nm, which correspond to (110) and ($11\bar{1}$), respectively (Figure 1). Only microscopically inclusion-free, optically clear, and homogeneous parts of the two samples were selected for high-pressure experiments. Additionally, colorless orthoclase was prepared for FTIR spectroscopic measurements of oriented polished plane-parallel plates (3 orientations: (001), (010), and (100)).

Table 1. Electron-microprobe chemical compositions of orthoclase (wt%).

Samples	SiO_2	Al_2O_3	Na_2O	K_2O	CaO	MgO	FeO	MnO	BaO	Or	Ab	An
colorless	55.97	27.53	6.19	10.03	0.01	0.06	0.05	0.02	0.01	51.6	48.3	0.1
pink	54.67	28.33	6.43	9.26	0.61	0.06	0.25	0.05	0.02	47.7	49.6	2.7

In the high-pressure experiments, samples were subjected to the desired pressure in a cubic zirconia anvil cell for 12 h before being analyzed by in situ Raman spectroscopy. After Raman spectroscopy analysis, the pressure was released slowly. Meanwhile, samples that were maintained at pressures around 300 MPa and 600 MPa were taken out from the

anvil for Fourier Transform Infrared (FTIR) spectroscopy analysis to evaluate the behavior of water in orthoclase.

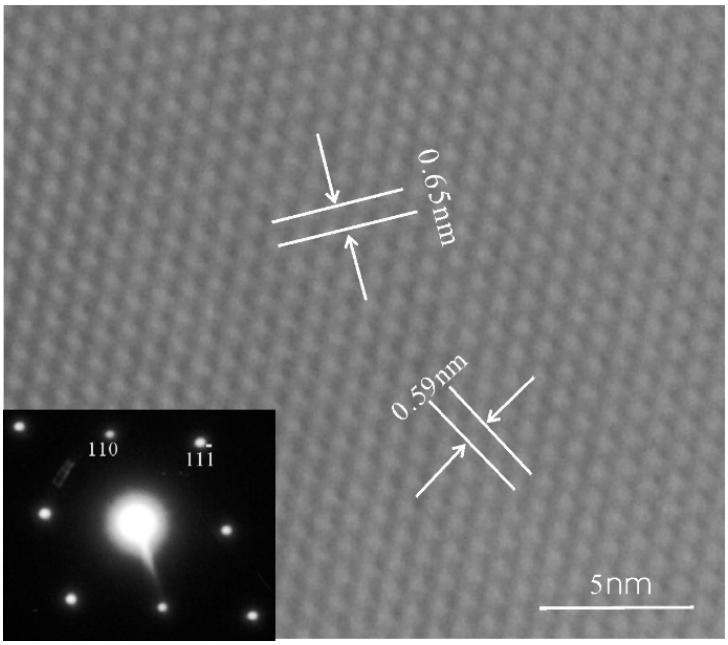

Figure 1. TEM image and electron diffraction pattern of colorless orthoclase.

2.2. Methods

CZ anvil cell. Metastable cubic zirconia (CZ) has been found to be inert, quite hard, and transparent to a large portion of the electromagnetic spectrum [27]. CZ anvil cell offers the advantage of a lower mid-IR cutoff point, enabling high-pressure experiments, and is a remarkable device for studying high-pressure crystallographic phenomena [27,28]. Cubic Zirconia (400 mg) for this study is a combination of ZrO_2 and HfO_2, containing 96.12 wt% and 3.88 wt%, respectively. High-pressure experiments in the CZ anvil cell were conducted using Cu gaskets with an initial thickness of 0.35 mm and a hole of 0.35 mm diameter. Pressure was measured using a quartz gauge as the pressure sensor. The force application was manual.

In the past several decades, 4:1 methanol–ethanol mixture has proven to be the most easily handled fluid used as a hydrostatic pressure-transmitting medium in connection with gasket cells [29–31]. Given the fact that the small molecular alcohols can enter the tunnels or structural cages of some microporous and mesoporous inorganic materials such as zeolites [32–34], it is reasonable that water can be used as a hydrostatic pressure fluid to study the tunnels of orthoclase. In this study, a 99.96% ions-free water was used as the pressure-transmitting medium.

Raman spectroscopy. In situ Raman spectroscopy together with a diamond cubic zirconia anvil cell was used to study the structural change at high pressures [35,36]. Raman spectra were collected on a Renishaw 1000 Raman microprobe spectrometer system coupled with a 20× microscope. To excite the samples, a continuous wave (CW) Ar ion laser with an incident laser power of 25 mW and a spot diameter of 1~2 μm was employed in the system. Raman scattering was detected in the range of 200–4000 cm^{-1} with a spectral resolution of ~1 cm^{-1}. The data collection time was 60 s.

The occurring depth of feldspar minerals in the lithosphere ranges from 10 to 20 km; thus, the corresponding pressure range of 300–600 MPa has been chosen to conduct the high-pressure experiment. Quartz is used in the high-pressure experiment as the standard to determine the pressures that the laboratory instrument applied on samples. The following functions derived by Schmidt and Ziemann [37] are used:

$$P = \frac{(\triangle v_p)_{464} - 2.051 \times 10^{-11} T^4 - 1.465 \times 10^{-8} T^3 + 1.801 \times 10^{-5} T^2 + 0.01216T - 0.29}{0.009} + 0.1 \quad (1)$$

$$\boldsymbol{p} = \mathbf{0.3}6079[(\Delta v_p)_{464}]^2 + 110.86(\Delta v_p)_{464}. \quad (2)$$

These functions are reliable when the shift does not exceed 20 cm^{-1}. The static hydropressures were obtained based on function (2).

FTIR spectroscopy. Fourier transform infrared spectra were measured using a Nicolet 750 Fourier-transform spectrometer. Prior to FTIR performance, samples were kept in a temperature control box at 180 °C for 3 h to free them of surface absorbent water. FTIR spectra were collected in the range of 1000–4000 cm^{-1}, with a resolution of 16 cm^{-1}. The beam was focused to form a ~100 μm spot on samples. For each spectrum, 128 scans were accumulated. FTIR spectra were collected in different crystallographic directions for colorless orthoclase.

3. Results

3.1. Raman Spectra with Increasing Pressure

The tectosilicate structure with fully linked tetrahedra generates a Raman spectral pattern distinctly different from those of chain, ortho-, ring, and layer silicates, in which the TO_4 tetrahedra are not linked at all, or are only partially linked, with other TO_4 units [38]. The strongest Raman peak of feldspars falls within the narrow region of 505 to 515 cm^{-1} (normally near ~510 cm^{-1}), which is distinctly different from those of other tectosilicates such as zeolites and quartz, whose strongest Raman peak is around 492 cm^{-1} and 464 cm^{-1}, respectively [37,39–41].

The Raman spectra of orthoclase were obtained under different pressures, ranging from 0.1 MPa to about 600 MPa. The pressure response of the orthoclase samples is depicted in Figure 2. With increasing pressure, Raman bands shift to higher wavenumbers, and the three peaks become gradually broader due to the decreasing lattice constants [42]. The relative intensities of bands show no significant changes under pressure, which is also observed in previous high-pressure Raman spectroscopy studies of other minerals [43,44].

Peaks between 450 and 520 cm^{-1} are attributed to the internal bending vibrational modes of the Si (Al^{IV})–O–Si bonds. The dominant feature of the orthoclase spectra is that the strongest peak in this region is near 510 cm^{-1} [40,45]. This peak is the most characteristic feldspar peak and is most frequently used to identify feldspar in the multi-phase spectra from igneous materials. Peaks between 600 and 800 cm^{-1} are assigned to the tetrahedral deformation modes [40,46]. The peak around 432 cm^{-1} is assigned to M–O bending or stretching vibrational modes [47]. Positions of the above three peaks (near 432, 510, and 800 cm^{-1}) are listed in Table 2. The peak around 507.27 cm^{-1} is shifted toward higher frequencies with increasing pressure (+2.19 cm^{-1} from 0.1 MPa to 606.87 MPa, equal to 3.61 cm^{-1}/GPa), as is the peak around 796.69 cm^{-1} (3.61 cm^{-1}/GPa). The peak around 432.33 cm^{-1} totally shifts 2.5 cm^{-1} (4.13 cm^{-1}/GPa) towards the higher wavenumber. The shifting to higher wavenumber in all three peaks means the chemical bonds become shorter under high pressures.

Table 2. Raman spectra data of colorless orthoclase at different pressures.

Wavenumber of quartz (cm^{-1})	464	465.10	466.73	467.56	468.60	469.38
Pressure (MPa)	0.1	122.38	305.34	399.23	517.59	606.87
M–O vibrational peak (cm^{-1})	432.33	433.02	433.20	433.50	433.50	434.83
Al^{IV}–O–Si vibrational peak (cm^{-1})	507.27	507.43	507.80	508.46	508.13	509.46
[SiO_4] vibrational peak (cm^{-1})	796.69	797.07	795.47	792.80	797.07	798.40

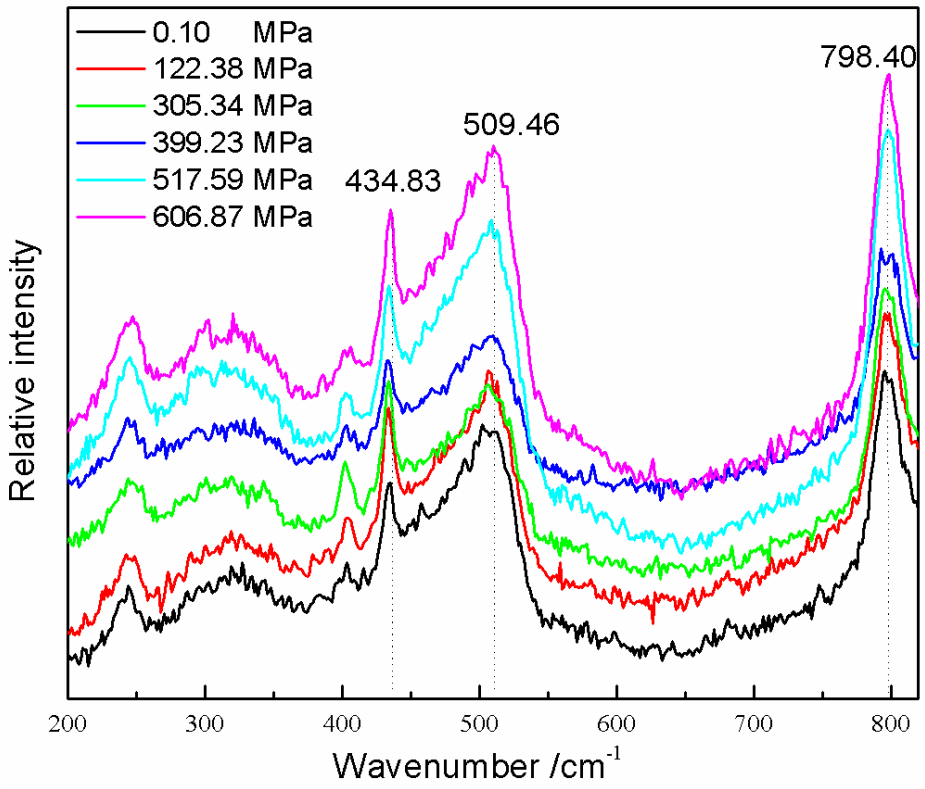

Figure 2. Raman spectra of colorless orthoclase at different pressures. The labelled numbers refer to the peak position at around 600 MPa pressure. The spectra are stacked for comparison.

3.2. FTIR Spectra with Increasing Pressure

Polarized spectra of orthoclase in the 1000–4000 cm^{-1} range are shown in Figure 3, and band positions are listed in Table 3. Although Galeener and Mikkelsen [48] proposed to quantify the H_2O content of silica glass at the ppm level with micro-Raman analytical procedures four decades ago, Freeman et al. [40] explained that the Raman peak positions of the felspars cannot be used to extract quantitative information due to the complex cation composition of the feldspar phases in comparison with olivine, pyroxene, and some Fe-oxides. Instead, micro-Fourier transform infrared spectroscopy is more efficient and the most widely used method to measure the hydrous absorbing species (including hydroxyl OH^- and molecular H_2O) and content, especially nominally anhydrous minerals with trace to minor amounts of hydrous components.

Table 3. FTIR spectra and analysis of two types of orthoclase at 300 and 600 MPa pressure.

Samples	Polarized Directions	Pressure	Wavenumber (cm^{-1})	Integral Absorbance * (cm^{-1})	Normalized Integral Absorbance * (cm^{-2})
Pink orthoclase	Perpendicular to (001)	1 atm	3420	17.98	1383
		300 MPa	3420	19.89	1904
		600 MPa	3410	20.92	2001
Colorless orthoclase	Perpendicular to (001)	1 atm	3420	1.50	120
		300 MPa	3310	11.32	1124
		600 MPa	3290	14.54	1570

* Note: Integral absorbance and Normalized integral absorbance are calculated based on 1 cm thickness.

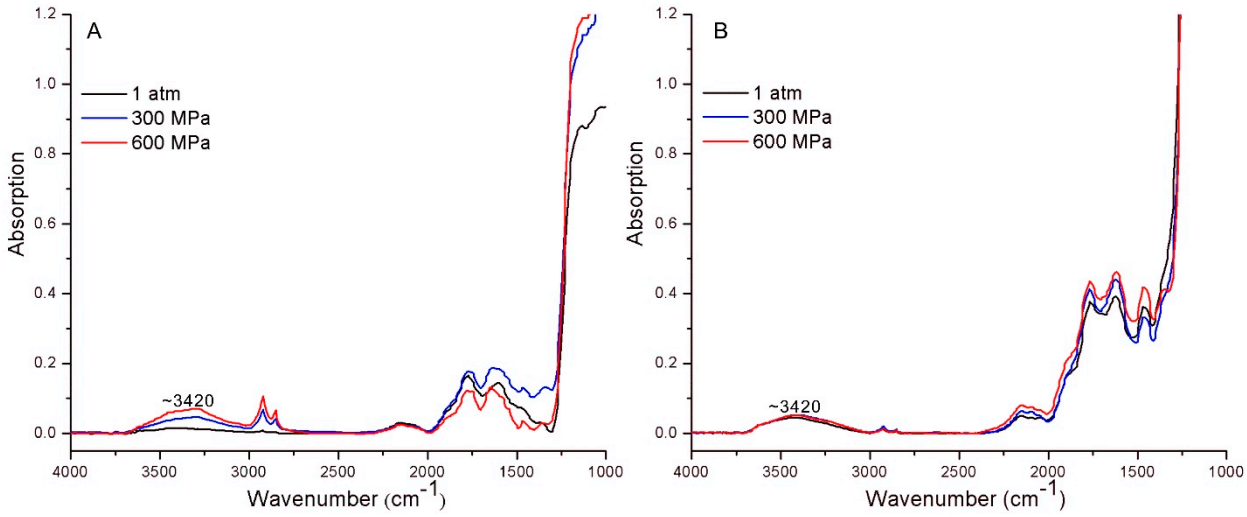

Figure 3. FTIR spectra of 300 and 600 MPa pressure: (**A**) colorless feldspar; (**B**) pink feldspar. The spectra are stacked for comparison.

The stretching bands of OH^- groups and the symmetric/asymmetric H_2O molecules occur between 4000 cm^{-1} and 2000 cm^{-1}. The most prominent absorption band produced by orthoclase crystals in this study is the broad symmetric peak centered at approximately 3420 cm^{-1} under 1 atmospheric pressure (1 atm) condition (Figure 3). For colorless orthoclase, the 3420 cm^{-1} peak shift to lower wavenumber, 3310 cm^{-1} at ~300 MPa and 3290 cm^{-1} at ~600 MPa, indicates that H_2O molecules are increased [49]. The remarkable observation is an intensity increase in H_2O broad band with increasing pressure of colorless orthoclase (Figure 3A). Statistically, integral absorbance increases sharply with pressure from 1 atm to 300 MPa, with only 1.50 cm^{-1} at 1 atm but 11.32 cm^{-1} at 300 MPa (Table 3). With pressure up to 600 MPa, the integral absorbance still rises slightly, to 14.54 cm^{-1} for colorless orthoclase. The normalized integral absorbance goes up to 1124 cm^{-2} and 1570 cm^{-2} at ~300 MPa and ~600 MPa, respectively, compared to only 120 cm^{-2} at 1 atm. The normalized integral absorbance is about 2.40 cm^{-2}/MPa, indicating that water goes into the channel of orthoclase under high pressures.

For pink orthoclase (Figure 3B), the integral absorbance increases gradually with no significant change in the position of peak (Table 3). The small increase in intensity is interpreted to reflect the existence of water in orthoclase. Little pressure dependence was observed between 300 MPa and 600 MPa. Doubling the pressure made a trace increase, which probably means the hydrous component is already saturated under 300 MPa pressure.

3.3. FTIR Spectra in Different Crystallography Direction at 1 atm

The FTIR spectra of colorless orthoclase collected from three different crystallography directions show differences in either position or intensity of peaks (Figure 4). Two groups of bands are observed in the spectra from 3000 cm^{-1} to 4000 cm^{-1}. The three different orientations, (001), (010), and (100), have a prominent broad band near 3418 cm^{-1}, which is in good agreement with those determined previously by Seaman et al. [50]. This peak is assigned to molecular H_2O [51]. The 3418 cm^{-1} band in the direction of (001) slightly shifts to 3420 cm^{-1} in (100) and (010) directions, indicating more molecular H_2O in the direction of (001) (Table 4). The intensity of this peak is very sensitive to the orientation of the orthoclase crystals. The 3418 cm^{-1} band has a stronger intensity in the direction of (001), compared to the other two directions (Figure 4). The normalized (to 1 cm thickness) integral absorbance in the direction of (001) is 1717.5 cm^{-2}, but the other two directions are much lower (Table 4). The differences in position and intensity of this peak in three different directions illustrate that the entrance of water into orthoclase structure has a preferred crystallographic

orientation. A small but sharp asymmetric band around 3619 cm^{-1} is obvious in the direction of (010), which is assigned to the OH^- stretching vibrational band [49].

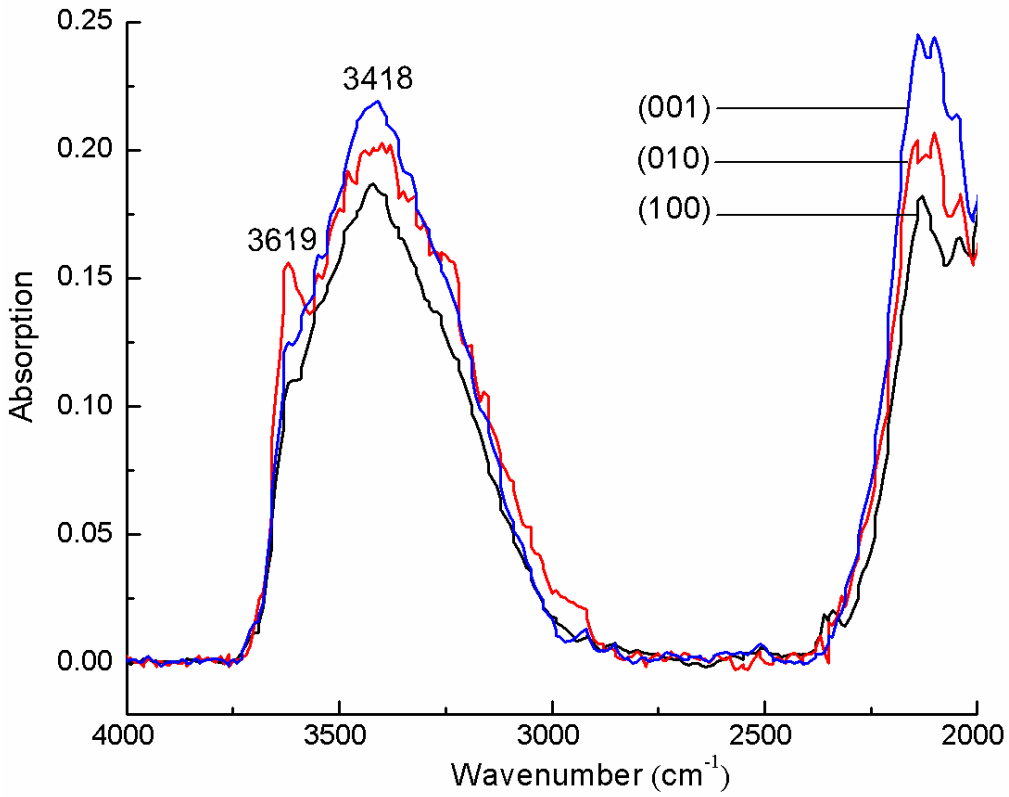

Figure 4. FTIR spectra of colorless orthoclase with the polarization direction of the IR radiation oriented perpendicular to (001), (010), and (100) vibration directions. The spectra are stacked for comparison.

Table 4. FTIR spectra and analysis of colorless orthoclase at 1 atm pressure.

Sample	Polarized Directions	Conditions	Wavenumber (cm^{-1})	Integral Absorbance * (cm^{-1})	Normalized Integral Absorbance * (cm^{-2})
Colorless Orthoclase	Nearly perpendicular to (100)	1 atm, room temperature	3420	18.19	1365.3
	Perpendicular to (010)		3420, 3619	19.40	1434
	Perpendicular to (001)		3418	20.86	1717.5

* Note: Integral absorbance and Normalized integral absorbance are calculated based on 1 cm thick.

4. Discussion

4.1. The Mechanism of Hydrogen in Feldspar

The idea that the hydrous species in alkali feldspar is mainly molecular H_2O whereas the plagioclase is OH^- has been proposed by several investigators. The hydrogen speciation in previously studied alkali feldspars, such as adularia [52,53], sanidine [53–55], microcline [55], anorthoclase [51,56] and orthoclase [51], are all mostly molecular H_2O, except for sanidine from Eifel in Germany, researched by Hofmeister and Rossman [55], deemed as OH^-. However, hydrogen in plagioclase mainly presents as OH^- [49,57]. Yang [58] found a good correlation between H solubility and K content, and he suggested a rough trend that H solubility increases with increasing K content from albite to labradorite

to anorthoclase. Smith [59] and Beran [60] tried to explain H_2O molecules in alkali feldspars as entering the M site of the structure. However, the M site is usually occupied by alkaline ions to balance the charge of aluminum (III) replacing silica (IV) and alkaline ions stay in fixed site. To facilitate the discussion, Figure 5A presents the crystallographic structure with K^+ in the M site in the channel along (101).

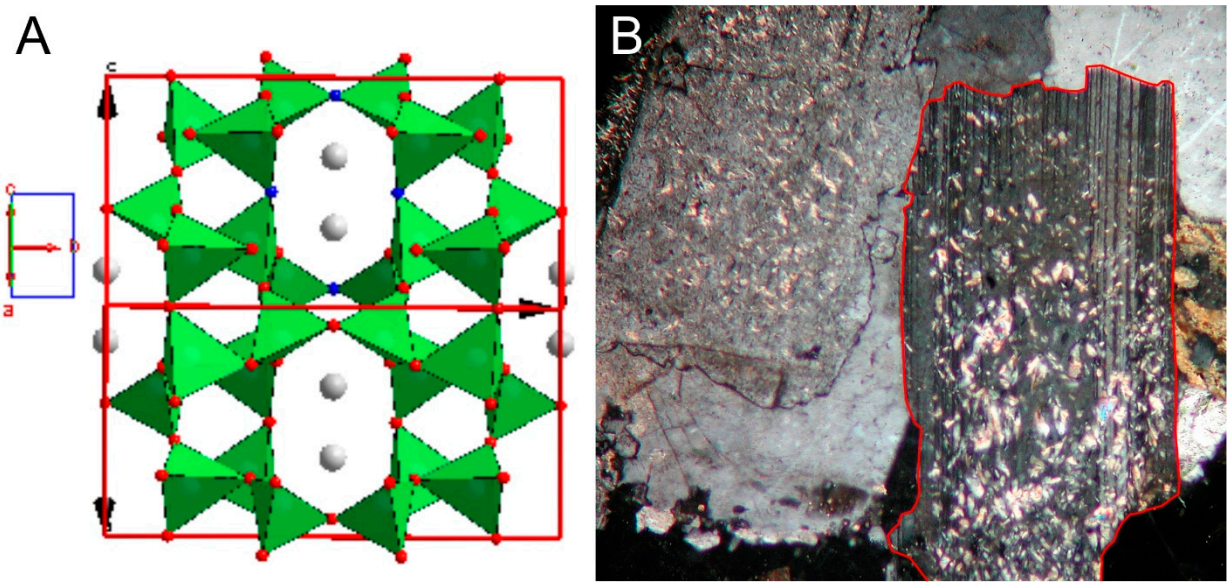

Figure 5. (**A**) Projection of the K-feldspar structure along the (101) direction with K (grey) in the channel; (**B**) sericitization alteration happened in the interior of K-feldspar crystal (e.g., red line).

A water molecule has a diameter of 0.276 nm, and its radius is 0.138 nm [61]. The order of ionic radius occupied in framework structure is K^+ (0.155 nm, coordination 9) > Na^+ (0.102 nm, coordination 6) > Ca^{2+} (0.100 nm, coordination 6) [62]. Considering the non-collapsible framework structure, large radius ions with high coordination can expand the aperture larger than those with relatively small ionic radius within limits. Baur and Joswig [63] explained the flexible but non-collapsible feldspar framework with individual T-O-T angles vary up to 27° without any significant effect on the overall mean T-O-T angle. Large ions prop up the apertures and result in crystallographic channels. Combing these properties together, it is reasonable to infer that K-feldspars have bigger channels than those of Na- or Ca-feldspar, which may allow molecular H_2O to enter.

4.2. The Speciation of Hydrogen in Orthoclase

This work presents detailed evidence of the behavior of hydrogen in orthoclase via various experimental techniques, especially the high-pressure method. With increasing pressure, Raman spectra present a shift toward higher wavenumber. Corner-sharing SiO_4 tetrahedra show positive relationships between a shorter SiO_4 bonding and a bigger force constant, which causes the shift toward the higher wavenumber [51,64]. In the present study, the chemical bonds of Si (Al^{IV})–O–Si become shorter with increasing pressures. Unfortunately, whether the presence of H_2O can lead to a higher wavenumber shift is not well studied in the literature.

The FTIR spectra at atmospheric pressure show orientation-dependent absorbance (Figure 4). As stated in the introduction, alkali feldspar minerals possess good ultra-micro channels, and the apertures of the channels also have crystallographic orientation. In this study, it is shown that there is a correlation between the intensity of FTIR spectra at atmospheric pressure and the aperture size of different orientations. Two peaks on the FTIR spectra in this study (3418 cm^{-1} and 3619 cm^{-1}, Table 4) are in good agreement with those previously studied bands (3400 cm^{-1} and 3630 cm^{-1}). Johnson and Rossman [49]

contributed these two peaks to molecular H_2O. Since it is difficult to prepare samples along the (101) direction, we could not collect the corresponding FTIR spectra. However, we expect higher intensity of molecular H_2O peak along the (101) direction based on the results of (001) and (100) (Figure 3).

In high-pressure experiments, the FTIR spectra of colorless orthoclase show good pressure-dependence. At atmospheric pressure, the peak still exists with very low intensity. With increasing pressure, more water in orthoclase raises the intensities which proves the possibility to make "H_2O" enter structural channels of orthoclase under certain hydrostatic pressure. The FTIR spectra intensities of pink orthoclase stay relatively stable with increasing pressure, illustrating a limit to the amount of water that can enter their structure via apertures or channels, especially if they are already saturated. The different responses to the pressure between colorless orthoclase and pink orthoclase might be related to the chemical compositions, with K_2O 10.03% and 9.26%, respectively (Table 1). Colorless orthoclase has a higher K content than that of pink orthoclase. The large radius of K can expand the aperture to become large enough to allow more water to enter. To point it out, this is just one possibility to explain the different responses to the pressure between colorless orthoclase and pink orthoclase based on our study.

4.3. Implications for Feldspar Alteration, Micropores/Microstructure, and Crustal Process

Sericitization is one of the most common types of hydrothermal alteration found in felsic rocks [65,66]. Sericitization of feldspars (including plagioclase) is one of the most ubiquitous characteristics of many granite-intrusive complexes [65,67]. An interesting phenomenon is that sericitization always occurs in an impregnated state in the interior of potassium feldspar crystals [23]. However, other alterations such as chloritization always occur along the crystal fringe of minerals such as pyroxene, hornblende, and biotite because these minerals have no channel structure to allow hydrothermal alteration to take place in the interior of the crystals. We propose that ultra-microchannels in potassium feldspar facilitate the entrance of H_2O molecules into their structure, leading to sericitization in the interior of potassium feldspar crystals. The reaction transpires as follows: $3KalSi_3O_8$ (potassium feldspar) + H_2O = $Kal_2AlSi_3O_{10}$ $(OH)_2$ (sericite) + $6SiO_2$ + K_2O. As shown in Figure 5B, the sericitization takes place in the interior of alkali feldspar. Moreover, sericitization also shows crystallographic orientation (Figure 5B).

Alkali feldspars with large-radius ions in the M sites might bring micropores and microstructures. Walker et al. [17] presented the size of micropores, from ~1μm to a few nm in length, typically 0.1 μm. Micropores or microtextures are contributed to the processes of crystals coarsening and deuteric or hydrothermal alteration. A process called 'unzipping', i.e., dissolution and reprecipitation around dislocation cores, is believed to result in turbid, microporous, and micropermeable feldspars (Parsons et al., 2000). Baur et al. [63] compared all feldspars with alkaline ions from the least open structure of $LiAlSi_3O_8$ to the most open structure of $RbAlSi_3O_8$. They found the non-collapsible nature of the feldspar-type aluminosilicate framework is because the T-O-T angles anti-rotate when a tetrahedron rotates upon compression or expansion in the framework in order to maintain open pores without expansion by inserted cations. Considering the non-collapsible frameworks achieving their non-collapsibility by being extremely flexible within certain limits, the replacement of K^+ with large ionic radius by those ions with small ionic radius such as Na^+ or Ca^{2+} is also mechanically allowed, resulting in compression of the framework. Consequently, the compression of the framework may lead to micropores and microstructures; however, these kinds of micropores and microstructures vary on a sub-micrometer scale due to the heterogeneous replacement. However, the TEM analysis shows that the studied feldspars are homogeneous and no microstructures are observed.

Feldspar is the most abundant constituent of the crust, mainly in the upper crust at the depth of 10–20 km (alkali feldspars can also form in more superficial conditions). Pressures ranging from 300 MPa to 600 MPa in this study correspond to the lithostatic pressures at those depths. On the surface of the crust, zeolite minerals contain water molecules in the

channels and cages of its framework structure. In the upper crust, alkali feldspars maintain trace amounts of molecular H_2O in its crystallographic channels. The apparent dependence of molecular H_2O on pressure in this study displays the importance of water in potassium feldspar in the upper crust. Although it saturates at a certain concentration and the overall water abundance in feldspar is small, the abundant feldspars content means the total mass of molecular water in the upper crust is potentially significant.

5. Conclusions

A high-pressure experiment coupled with FTIR spectroscopy of orthoclase provides evidence of water entering ultra-microchannels in feldspar structure. With increasing pressure, colorless orthoclase exhibits higher peak intensities of water in the FTIR spectra. The normalized integral absorbance increases up to 1124 cm^{-2} and 1570 cm^{-2} at ~300 MPa and ~600 MPa, respectively, compared to only 120 cm^{-2} at 1 atm. An orientation-dependent FTIR reveals the preference of orientation when water enters the structure of orthoclase. Nearly perpendicular to (001) is preferred, with the highest normalized integral absorbance in this study (1717.5 cm^{-2}). Water in the ultra-microchannels excellently explains the phenomenon that sericitization always occurs in an impregnated state in the interior of potassium feldspar crystals. This study provides a mechanism for feldspar alteration and important insights into the behavior of water molecules in nominally anhydrous minerals in the upper crust of the Earth.

Author Contributions: Writing—original draft preparation: H.Z.; investigation: R.L. and H.Z.; writing—review and editing: H.Z. and A.L. All authors have read and agreed to the published version of the manuscript.

Funding: This work was funded by the Science and Technology Development Fund, Macau SAR (File no. SKL-LPS(MUST)-2021-2023) and the Natural Science Foundation of China (no. 41820104003 & 41172043).

Institutional Review Board Statement: Not applicable.

Informed Consent Statement: Not applicable.

Data Availability Statement: Data are contained within the article.

Acknowledgments: Technical comments and English review by Sky P. Beard are appreciated. Constructive reviews by anonymous reviewers were very helpful in revising the manuscript.

Conflicts of Interest: The authors declare no conflict of interest.

References

1. Yuan, G.; Cao, Y.; Schulz, H.-M.; Hao, F.; Gluyas, J.; Liu, K.; Yang, T.; Wang, Y.; Xi, K.; Li, F. A review of feldspar alteration and its geological significance in sedimentary basins: From shallow aquifers to deep hydrocarbon reservoirs. *Earth-Sci. Rev.* **2019**, *191*, 114–140. [CrossRef]
2. Parsons, I. *Feldspars and Their Reactions*; Springer Science & Business Media: Berlin/Heidelberg, Germany, 2012.
3. Solé, J.; Pi-Puig, T.; Ortega-Rivera, A. A Mineralogical, Geochemical, and Geochronological Study of 'Valencianite' from La Valenciana Mine, Guanajuato, Mexico. *Minerals* **2021**, *11*, 741. [CrossRef]
4. Machatschki, F. The structure and constitution of feldspars. *Centr. Min. Abt. A* **1928**, *8*, 97–104.
5. Jones, J. Order in alkali feldspars. *Nature* **1966**, *210*, 1352–1353. [CrossRef]
6. Stewart, D.; Ribbe, P. Structural explanation for variations in cell parameters of alkali feldspar with Al/Si ordering. *Am. J. Sci.* **1969**, *267*, 444–462.
7. Taylor, W.H.; Darbyshire, J.A.; Strunz, H. An X-ray investigation of the feldspars. *ZK* **1934**, *87*, 35.
8. Deer, W.A.; Howie, R.; Zussman, J. *Rock-Forming Minerals, Volume 4A: Framework Silicates–Feldspars*; The Geological Society: London, UK, 2001; Volume viii, p. 972.
9. Smith, J.V. *Feldspar Minerals: Crystal Structure and Physical Properties 1*; Springer Science & Business Media: Berlin/Heidelberg, Germany, 2013.
10. Smith, J.V. *Feldspar Minerals: In Three Volumes. 2. Chemical and Textural Properties*; Springer: Berlin/Heidelberg, Germany, 1974.
11. Brown, W.L. *Feldspars and Feldspathoids: Structures, Properties and Occurrences*; Springer Science & Business Media: Berlin/Heidelberg, Germany, 2013.

12. Lu, A.; Huang, S.; Liu, R.; Zhao, D.; Qin, S. Environmental Effects of Micro- and Ultra-microchannel Structures of Natural Minerals. *Acta Geol. Sin.-Engl. Ed.* **2006**, *80*, 161–169.
13. Shamloo, H.I.; Till, C.B.; Hervig, R.L. Multi-mode magnesium diffusion in sanidine: Applications for geospeedometry in magmatic systems. *Geochim. Cosmochim. Acta* **2021**, *298*, 55–69. [CrossRef]
14. Dietrich, R. K-feldspar structural states as petrogenetic indicators. *Nor. Geol. Tidsskr. Bind.* **1962**, *42*, 394–414.
15. Ragland, P.C. Composition and structural state of the potassic phase in perthites as related to petrogenesis of a granitic pluton. *Lithos* **1970**, *3*, 167–189. [CrossRef]
16. Parsons, I.; Gerald, J.D.F.; Lee, M.R. Routine characterization and interpretation of complex alkali feldspar intergrowths. *Am. Mineral.* **2015**, *100*, 1277–1303. [CrossRef]
17. Walker, F.D.L.; Lee, M.R.; Parsons, I. Micropores and micropermeable texture in alkali feldspars: Geochemical and geophysical implications. *Mineral. Mag.* **1995**, *59*, 505–534. [CrossRef]
18. Mamonov, A.; Puntervold, T.; Strand, S.; Hetland, B.; Andersen, Y.; Wealth, A.; Nadeau, P.H. Contribution of feldspar minerals to pH during Smart Water EOR processes in sandstones. *Energy Fuels* **2019**, *34*, 55–64. [CrossRef]
19. Yun, J.; Kumar, A.; Removski, N.; Shchukarev, A.; Link, N.; Boily, J.-F.; Bertram, A.K. Effects of Inorganic Acids and Organic Solutes on the Ice Nucleating Ability and Surface Properties of Potassium-Rich Feldspar. *ACS Earth Space Chem.* **2021**, *5*, 1212–1222. [CrossRef]
20. Choudhary, A.; Khandelwal, N.; Singh, N.; Tiwari, E.; Ganie, Z.A.; Darbha, G.K. Nanoplastics interaction with feldspar and weathering originated secondary minerals (kaolinite and gibbsite) in the riverine environment. *Sci. Total Environ.* **2022**, *818*, 151831. [CrossRef] [PubMed]
21. Wollast, R. Kinetics of the alteration of K-feldspar in buffered solutions at low temperature. *Geochim. Cosmochim. Acta* **1967**, *31*, 635–648. [CrossRef]
22. Duan, G.; Ram, R.; Xing, Y.; Etschmann, B.; Brugger, J. Kinetically driven successive sodic and potassic alteration of feldspar. *Nat. Commun.* **2021**, *12*, 4435. [CrossRef]
23. Engelhardt, W.V.; Matthäi, S.K.; Walzebuck, J. Araguainha impact crater, Brazil. I. The interior part of the uplift. *Meteoritics* **1992**, *27*, 442–457. [CrossRef]
24. Wibberley, C. Are feldspar-to-mica reactions necessarily reaction-softening processes in fault zones? *JSG* **1999**, *21*, 1219–1227. [CrossRef]
25. Kawano, M.; Tomita, K. Formation of mica during experimental alteration of K-feldspar. *Clays Clay Miner.* **1995**, *43*, 397–405. [CrossRef]
26. Garrels, R.; Howard, P. Reactions of feldspar and mica with water at low temperature and pressure. *Clays Clay Miner.* **1957**, *6*, 68–88. [CrossRef]
27. Patterson, D.E.; Margrave, J.L. The use of gem-cut cubic zirconia in the diamond anvil cell. *J. Phys. Chem.* **1990**, *94*, 1094–1096. [CrossRef]
28. Chen, J.; Zheng, H.; Xiao, W.; Zeng, Y. High-temperature and high-pressure cubic zirconia anvil cell for Raman spectroscopy. *Appl. Spectrosc.* **2003**, *57*, 1295–1299. [CrossRef] [PubMed]
29. Grocholski, B.; Jeanloz, R. High-pressure and-temperature viscosity measurements of methanol and 4: 1 methanol: Ethanol solution. *J. Chem. Phys.* **2005**, *123*, 204503. [CrossRef]
30. Eggert, J.H.; Xu, L.; Che, R.; Chen, L.; Wang, J. High pressure refractive index measurements of 4: 1 methanol: Ethanol. *J. Appl. Phys.* **1992**, *72*, 2453–2461. [CrossRef]
31. Lemos, V.; Camargo, F. Effects of pressure on the Raman spectra of a 4: 1 methanol–ethanol mixture. *J. Raman Spectrosc.* **1990**, *21*, 123–126. [CrossRef]
32. Hazen, R. Zeolite molecular sieve 4A: Anomalous compressibility and volume discontinuities at high pressure. *Science* **1983**, *219*, 1065–1067. [CrossRef]
33. Lee, Y.; Vogt, T.; Hriljac, J.A.; Parise, J.B.; Hanson, J.C.; Kim, S.J. Non-framework cation migration and irreversible pressure-induced hydration in a zeolite. *Nature* **2002**, *420*, 485–489. [CrossRef]
34. Angel, R.J.; Bujak, M.; Zhao, J.; Gatta, G.D.; Jacobsen, S.D. Effective hydrostatic limits of pressure media for high-pressure crystallographic studies. *J. Appl. Crystallogr.* **2007**, *40*, 26–32. [CrossRef]
35. Goncharov, A.F. Raman spectroscopy at high pressures. *Int. J. Spectrosc.* **2012**, *2012*, 617528. [CrossRef]
36. Sharma, S.K. Raman spectroscopy at very high pressures. *Raman Scatt. Lumin. Spectrosc. Instrum. Technol.* **1989**, *1055*, 105–116.
37. Schmidt, C.; Ziemann, M.A. In-situ Raman spectroscopy of quartz: A pressure sensor for hydrothermal diamond-anvil cell experiments at elevated temperatures. *Am. Mineral.* **2000**, *85*, 1725–1734. [CrossRef]
38. Deer, W.A. *Rock-Forming Minerals*. 2011. Available online: https://books.google.co.uk/books?hl=zh-CN&lr=lang_en&id=2GLGx6A0d0UC&oi=fnd&pg=PR5&dq=Rock-Forming+Minerals&ots=o-Nx3qJx35&sig=yh_WekveZ2g6e7JZvFCvlhnOiKE#v=onepage&q&f=false (accessed on 6 June 2022).
39. Mernagh, T. Use of the laser Raman microprobe for discrimination amongst feldspar minerals. *J. Raman Spectrosc.* **1991**, *22*, 453–457. [CrossRef]
40. Freeman, J.J.; Wang, A.; Kuebler, K.E.; Jolliff, B.L.; Haskin, L.A. Characterization of natural feldspars by Raman spectroscopy for future planetary exploration. *Can. Mineral.* **2008**, *46*, 1477–1500. [CrossRef]

41. Sharma, S.K.; Simons, B.; Yoder, H. Raman study of anorthite, calcium Tschermak's pyroxene, and gehlenite in crystalline and glassy states. *Am. Mineral.* **1983**, *68*, 1113–1125.
42. Ostertag, R. Shock experiments on feldspar crystals. *J. Geophys. Res. Solid Earth* **1983**, *88*, B364–B376. [CrossRef]
43. Kyono, A.; Ahart, M.; Yamanaka, T.; Gramsch, S.; Mao, H.-k.; Hemley, R.J. High-pressure Raman spectroscopic studies of ulvospinel Fe_2TiO_4. *Am. Mineral.* **2011**, *96*, 1193–1198. [CrossRef]
44. Ruiz-Fuertes, J.; Errandonea, D.; López-Moreno, S.; González, J.; Gomis, O.; Vilaplana, R.; Manjón, F.; Muñoz, A.; Rodríguez-Hernández, P.; Friedrich, A. High-pressure Raman spectroscopy and lattice-dynamics calculations on scintillating $MgWO_4$: Comparison with isomorphic compounds. *Phys. Rev. B* **2011**, *83*, 214112. [CrossRef]
45. Tan, J.; Zhao, S.; Huang, Q.; Davies, G.; Mo, X. The microstructure of silicate varying with crystal and melt properties under the same cooling condition. *Mater. Res. Bull.* **2004**, *39*, 939–948. [CrossRef]
46. Holtz, F.; Bény, J.-M.; Mysen, B.O.; Pichavant, M. High-temperature Raman spectroscopy of silicate and aluminosilicate hydrous glasses: Implications for water speciation. *Chem. Geol.* **1996**, *128*, 25–39. [CrossRef]
47. Makreski, P.; Jovanovski, G.; Kaitner, B. Minerals from Macedonia. XXIV. Spectra-structure characterization of tectosilicates. *J. Mol. Struct.* **2009**, *924*, 413–419. [CrossRef]
48. Galeener, F.L.; Mikkelsen, J., Jr. Vibrational dynamics in ^{18}O-substituted vitreous SiO_2. *Phys. Rev. B* **1981**, *23*, 5527. [CrossRef]
49. Johnson, E.A.; Rossman, G.R. A survey of hydrous species and concentrations in igneous feldspars. *Am. Mineral.* **2004**, *89*, 586–600. [CrossRef]
50. Seaman, S.J.; Dyar, M.D.; Marinkovic, N.; Dunbar, N.W. An FTIR study of hydrogen in anorthoclase and associated melt inclusions. *Am. Mineral.* **2006**, *91*, 12–20. [CrossRef]
51. Wilkins, R.; Sabine, W. Water content of some nominally anhydrous silicates. *Am. Mineral. J. Earth Planet. Mater.* **1973**, *58*, 508–516.
52. Kronenberg, A.K.; Yund, R.A.; Rossman, G.R. Stationary and mobile hydrogen defects in potassium feldspar. *Geochim. Cosmochim. Acta* **1996**, *60*, 4075–4094. [CrossRef]
53. Lehmann, G. *Spectroscopy of Feldspars. Feldspars and Feldspathoids*; Springer: Berlin/Heidelberg, Germany, 1984; pp. 121–162.
54. Hofmeister, A.M.; Rossman, G.R. A spectroscopic study of irradiation coloring of amazonite: Structurally hydrous, Pb-bearing feldspar. *Am. Mineral.* **1985**, *70*, 794–804.
55. Hofmeister, A.M.; Rossman, G.R. A model for the irradiative coloration of smoky feldspar and the inhibiting influence of water. *Phys. Chem. Miner.* **1985**, *12*, 324–332. [CrossRef]
56. Xia, Q.; Pan, Y.; Chen, D.; Kohn, S.; Zhi, X.; Guo, L.; Cheng, H.; Wu, Y. Structural water in anorthoclase megacrysts from alkalic basalts: FTIR and NMR study. *Acta Petrol. Sin.* **2000**, *16*, 485–491.
57. Rossman, G. Studies of OH in nominally anhydrous minerals. *Phys. Chem. Miner.* **1996**, *23*, 299–304. [CrossRef]
58. Yang, X. An experimental study of H solubility in feldspars: Effect of composition, oxygen fugacity, temperature and pressure and implications for crustal processes. *Geochim. Cosmochim. Acta* **2012**, *97*, 46–57. [CrossRef]
59. Smith, J.V. *Feldspar Minerals: 2 Chemical and Textural Properties*; Springer Science & Business Media. Available online: https://books.google.co.uk/books?hl=zh-CN&lr=lang_en&id=IObtCAAAQBAJ&oi=fnd&pg=PA3&dq=Feldspar+Minerals:+2+Chemical+and+Textural+Properties%3B+Springer+Science+%26+Business+Media&ots=RTL4w_rdrJ&sig=OqHau4WuboNuzeH2ooV_zwtKlOc#v=onepage&q=Feldspar%20Minerals%3A%202%20Chemical%20and%20Textural%20Properties%3B%20Springer%20Science%20%26%20Business%20Media&f=false (accessed on 5 June 2022).
60. Beran, A. A model of water allocation in alkali feldspar, derived from infrared-spectroscopic investigations. *Phys. Chem. Miner.* **1986**, *13*, 306–310. [CrossRef]
61. Marcus, Y. On Water Structure in Concentrated Salt Solutions. *J. Solut. Chem.* **2009**, *38*, 513–516. [CrossRef]
62. Shannon, R.D. Revised effective ionic radii and systematic studies of interatomic distances in halides and chalcogenides. *Acta Crystallogr. Sect. A Cryst. Phys. Diffr. Theor. Gen. Crystallogr.* **1976**, *32*, 751–767. [CrossRef]
63. Baur, W.H.; Joswig, W.; Müller, G. Mechanics of the feldspar framework; Crystal structure of Li-feldspar. *J. Solid State Chem.* **1996**, *121*, 12–23. [CrossRef]
64. Hemley, R.; Mao, H.; Bell, P.; Mysen, B. Raman spectroscopy of SiO_2 glass at high pressure. *Phys. Rev. Lett.* **1986**, *57*, 747. [CrossRef]
65. Que, M.; Allen, A.R. Sericitization of plagioclase in the Rosses granite complex, Co. Donegal, Ireland. *Mineral. Mag.* **1996**, *60*, 927–936. [CrossRef]
66. Zuo, H.; Lu, A.; Gu, X.; Ma, W.; Cui, Y.; Yi, L.; Lei, H.; Wang, Z.; Zhang, D.; Liu, J. Typomorphic feature of chromium sericite in granite hosted gold deposits in Jiaodong Peninsula, China. *Appl. Clay Sci.* **2016**, *119*, 49–58. [CrossRef]
67. Verati, C.; Jourdan, F. Modelling effect of sericitization of plagioclase on the 40K/40Ar and 40Ar/39Ar chronometers: Implication for dating basaltic rocks and mineral deposits. *Geol. Soc. Lond. Spec. Publ.* **2014**, *378*, 155–174. [CrossRef]